Beta 1 Integrin Signaling Mediates Pancreatic Ductal Adenocarcinoma Resistance to MEK Inhibition

Arthur Brannon III[1*], Donovan Drouillard[2*], Nina Steele[3*], Shadae Sutherland[2], Howard C. Crawford[4,5] and Marina Pasca di Magliano[2,3,6]

[1] Medical Scientist Training Program, University of Michigan, Ann Arbor, United States

[2] Department of Surgery, University of Michigan, Ann Arbor, United States

[3] Department of Cell and Developmental Biology, University of Michigan, Ann Arbor, United States

[4] Department of Molecular and Integrative Physiology, University of Michigan, Ann Arbor, United States

[5] Department of Internal Medicine, University of Michigan, Ann Arbor, United States

[6] Rogel Cancer Center, University of Michigan, Ann Arbor, United States

*these authors equally contributed to this work

Correspondence:

Marina Pasca di Magliano Ph.D.

University of Michigan Cancer Center, Department of Surgery, 1500 East Medical Center Drive, Cancer Center Room 6110. Ann Arbor, Michigan 48109-0944, United States

Tel: (734) 763-3950. Marinapa@umich.edu

Short title: Beta-1 Integrin and MEK in Pancreatic Cancer

Grants: American Cancer Society, NIH P30CA46592, NIH R01CA151588, NIH R01CA198074, NIH U01CA224145

Abstract

Pancreatic cancer, one of the deadliest human malignancies, has a dismal 5-year survival rate of 9%. The high mortality rate can be attributed to multiple factors, including late diagnosis and lack of effective therapies. *KRAS* is the most commonly mutated gene in pancreatic cancer, but clinical agents that directly target mutant KRAS are not available. Several effector pathways are activated downstream of oncogenic Kras, including MAPK signaling. MAPK signaling can be inhibited by targeting MEK1/2; unfortunately, this approach has been largely ineffective in pancreatic cancer. Here, we set out to identify mechanisms of MEK inhibitor resistance in pancreatic cancer using primary mouse and human 3D organoid cultures. We optimized the culture of pancreatic tumor organoids that utilized Matrigel as a basement membrane mimetic, facilitating polarized growth. Pancreatic tumor organoids recapitulated mutant KRAS dependency and recalcitrance to MEK inhibition. Treatment of the organoids with trametinib, a MEK inhibitor, had only a modest effect on these cultures. We observed that cells adjacent to the basement membrane mimetic Matrigel survived MEK inhibition, while the cells in the interior layers underwent apoptosis. Our findings suggested that basement membrane attachment provided survival signals. We thus targeted integrin β1, a mediator of extracellular matrix contact, and found that combined MEK and integrin β1 inhibition bypassed trametinib resistance. Our data support exploring integrin signaling inhibition as a component of combination therapy in pancreatic cancer.

Introduction

Pancreatic Ductal Adenocarcinoma (PDAC), accounting for 90% of pancreatic neoplasms, is projected to become the 2nd leading cause of cancer death in the US by 2030 [1,2]. Almost 95% of PDAC cases express a mutated form of the GTPase KRAS [3]. Activating mutations in *KRAS* (the most prevalent being $KRAS^{G12D}$), lead to constitutive, aberrant activation of KRAS and subsequent neoplasia [4]. The Mitogen-

42 activated protein kinase (MAPK) pathway is a downstream effector of oncogenic KRAS and its activation
43 promotes cell growth, survival, and proliferation [5]. While KRAS inhibitors are currently not available,
44 the MAPK signaling pathway can be targeted by multiple FDA-approved agents, many of which target
45 the key kinases MEK1/2 [6, 7]. Inhibition of MAPK signaling blocks the onset of carcinogenesis [8],
46 possibly by interfering with the dedifferentiation of acinar cells to duct-like cells that are susceptible to
47 transformation, a process known as acinar-ductal metaplasia (ADM). MEK inhibition has been tested in
48 pancreatic cancer as a single-agent therapy, as well as in combination with Phosphoinositide Kinase-3
49 (PI3K) pathway inhibition (targeting another downstream effector of KRAS [9, 10]). Unfortunately, these
50 efforts have failed to demonstrate clinical benefit [11].

51

52 MEK inhibition using trametinib is tolerated in the PDAC patient population [10]. We set out to
53 understand mechanisms of resistance to trametinib with the goal to identify potential new combination
54 approaches for pancreatic cancer therapy. Since the resistance to trametinib is observed in tumor cells
55 in isolation, we focused here on the cell-autonomous mechanisms of resistance, using a three
56 dimensional (3D) *in vitro* model of PDAC. In this study, we found that cells adjacent to the basement
57 membrane exhibit a survival advantage over cells lacking ECM signaling when administered a MEK
58 inhibitor. Furthermore, KRAS effector signaling is reduced to only ECM-adjacent cells when given an β1
59 integrin neutralizing antibody. Lastly, dual blockade of both MEK and β1 integrin significantly increased
60 PDAC cell apoptosis compared to singular inhibition of MEK or β1 integrin. These results indicate that β1
61 integrin plays an important role in mediating PDAC resistance to MEK inhibition.

62

63 **Results**

64 **Establishing a 3D culture model of pancreatic cancer.**

65 The iKras*;p53* mouse model of pancreatic cancer mimics the progression of the human disease [12]. In
66 this model, oncogenic Kras^{G12D} (Kras*) expression is regulated by a tet-response element, while mutant
67 p53^{R172H} is constitutively expressed in the pancreas, allowing for inducible and reversible expression of
68 Kras* upon administration or removal of doxycycline (DOX), respectively (Fig. 1a). The generation of cell
69 lines from primary tumors formed in iKras*;p53* pancreata was previously described [13].
70 Subsequently, iKras*;p53* PDAC cells were passaged and maintained in two-dimensional culture in
71 presence of DOX to maintain expression of oncogenic Kras (Fig. 1b).

72

73 Growth in 3D was achieved by trypsinizing and resuspending PDAC cells in single-cell-suspension with
74 cell culture medium that contained DOX and solubilized Growth Factor Reduced (GFR) Matrigel, a
75 basement membrane mimetic comprised of extracellular matrix (ECM) proteins: laminins, Type IV
76 collagen (Col4), and entactin. Matrigel facilitates 3D proliferation and adhesion of cells, interactions that
77 may regulate crucial aspects of cancer molecular pathogenesis *in vivo* [14]. Subsequently, PDAC cells in
78 suspension were plated atop a layer of solidified GFR Matrigel. Approximately 6 days following plating,
79 PDAC cells organized into 3D, discrete clusters that were fixed for histochemical analysis (Fig. 1c-e). To
80 determine whether cells in this 3D assay recapitulated oncogenic Kras* dependency observed in vivo,
81 cells were randomized into two experimental groups: DOX was either withheld or administered to the
82 media at the time of plating to inactivate or activate oncogenic Kras* expression, respectively.
83 Brightfield microscopy was used to monitor cell growth and ImageJ was used to measure PDAC cluster
84 area (Supplementary Fig. 1). DOX administration induced an approximate 4-fold increase in average
85 cluster area (Fig. 1f, g, Supplementary Fig. 2), indicating that oncogenic Kras* expression was sufficient
86 to facilitate tumor cell growth and proliferation in this model. These results are consistent with previous
87 *in vivo* and *in vitro* findings [13].

88

89 In 2D, oncogenic Kras had a limited effect on cell viability (Supplementary Fig. 3). Conversely, #D growth
90 was dependent on the expression of oncogenic Kras (Supplementary Fig. 2), mimicking the requirement
91 for oncogenic Kras *in vivo*. We used the 3D system to study the effect of inhibiting Kras* downstream
92 effector pathways, specifically MAPK and PI3K, in the tumor cells. First, we performed immunostaining
93 on iKras*p53* PDAC clusters grown in the presence of DOX for 6 days. Similar to human PDAC and tissue
94 from the primary iKras*p53* tumor (Fig. 2 a, b), iKras*p53* PDAC cells in 3D culture upregulated
95 phosphorylated ERK (pERK) (Fig. 2a) and phosphorylated S6 (pS6) (Fig. 2b), indicating activation of the
96 MAPK and PI3K pathway, respectively. Furthermore, we observed expression of membrane proteins E-
97 Cadherin and Claudin-18 (Fig. 2c-j), both epithelial cell markers. Taken together, these data suggest two
98 implications for our system. First, iKras*p53* PDAC cells in our 3D culture system recapitulate common
99 biological characteristics of human PDAC and other murine *in vivo* models. Second, it can be used to
100 study the effect of signaling pathways in a system that mimics the spatial relationships of tumor cells,
101 while allowing us to dissect signaling, in absence of the complexity of the microenvironment.

102

103 **MEK inhibition inhibits PDAC growth in 3D and induces apoptotic lumen formation**

104 To inhibit MAPK signaling, clusters were grown for 6 days and then administered PD325901 (MEK
105 inhibitor, abbreviated MEKi-P) for 4 days; DOX was present in the media at all points, so that oncogenic
106 Kras* was constitutively expressed. Administration of the inhibitor was sufficient to abrogate Kras*-
107 mediated cluster growth (Fig. 3a-e). Upon histologic analysis we found that MEK inhibition decreased
108 the expression of pERK, suggesting successful inactivation of the MAPK signaling pathway (Fig. 3f-i).
109 However, similar to the in vivo situation, cultures survived, indicating resistance to MEK inhibition. The
110 MEK-resistant cells formed single-layer clusters, while the lumen (occupying >75% of cross-section area)

111 contained apoptotic debris. This finding was dose-dependent (Fig. 3j), as increasing concentration of
112 MEKi led to increased prevalence of single-layered clusters with large lumens. These results suggested
113 that cells at the periphery of the cluster, and thus in contact with the basement membrane, were
114 uniquely resistant to MEK inhibition. Intriguingly, this finding recapitulated what we and others
115 observed in vivo upon inactivation of oncogenic Kras [13, 15].

116

117 To confirm this initial finding with a different MEK inhibitor, PDAC cells were grown for 1 week and
118 administered a clinically available MEK inhibitor, trametinib (MEKi-T) for 4 days. To visualize any
119 morphologic changes induced by MEK inhibition, PDAC clusters were fixed, sectioned, and stained for
120 hematoxylin and eosin. Similar to clusters treated with MEKi-P, MEKi-T treated clusters were found to
121 have an apoptotic lumen-- evidenced by unorganized hyaline aggregation as well hyperchromatic debris,
122 which indicates nuclear fragmentation, features consistent with cells that undergo programmed cell
123 death (Fig. 4c). The prevalence of clusters with apoptotic debris that occupied >75% of a single lumen
124 was found to be significantly increased approximately 7-fold following MEK-T administration (Fig. 4d). To
125 establish that the cells had indeed undergone apoptosis, we stained sections of PDAC clusters for
126 cleaved caspase-3 (CC3) (Fig. 4a, b). Thus, using two different MEK inhibitors, we showed that cancer
127 cells vary in their sensitivity to MEK inhibition.

128

129 **PDAC cells adjacent to Matrigel display a survival advantage**

130 The prevalence of single-layer cluster morphology suggests that cells in contact with the Matrigel
131 basement membrane mimetic have a survival advantage. In this 3D system, Matrigel coats the entire
132 outside of the cluster *in vitro*, so following fixation and sectioning, the outermost layer of cells in cluster
133 cross-sections are considered adjacent to the Matrigel (Supplementary Fig. 1). This can be visualized by

134 staining for Type IV collagen (Col4), a primary component of Matrigel and the basement membrane *in*
135 *vivo*. Staining reveals Col4 enrichment on the outer edge of clusters treated with either vehicle (DMSO)
136 or MEKi-T, suggesting that MEK inhibition does not affect organization of basement membrane (Fig. 5a).
137 Upon quantification of cells adjacent or nonadjacent to Matrigel, the MEK-T treated clusters showed an
138 increased prevalence of cells adjacent to the Matrigel, suggesting that these cells have a survival
139 advantage over cells that lack ECM attachment (Fig. 5b). The phenomenon of anoikis, a form of
140 programmed cell death in response to loss of ECM signaling, is well described in other systems. [16]. We
141 hypothesized that Matrigel-adjacent cells were able to resist anoikis due to their ability to interact and
142 exchange signals with ECM components.

143

144 Human and murine PDAC cells have been shown to engage in complex signaling with the surrounding
145 microenvironment, yet the implications of this signaling and their effects on disease pathogenesis are
146 currently poorly understood. In multiple systems, the transmembrane, bidirectional signaling molecule
147 β1 integrin has been implicated in coordinating cell-to-cell and cell-to-ECM interactions [17]. And in the
148 normal pancreas, β1 integrin expression is necessary for acinar maintenance [18]. In our 3D system, we
149 found that iKras*p53* PDAC cells expressed β1 integrin (Supplementary Fig. 4), and this expression was
150 not affected by administration of MEKi-T (Supplementary Fig. 4). Given that Matrigel-adjacent PDAC
151 cells show a survival advantage and express β1 integrin, we hypothesized that β1 integrin signaling
152 mediated survival in this population.

153

154 **Beta-1 integrin inhibition disrupted cell:cell organization and decreased Kras effector signaling**

155 The function of β1 integrin is highly dependent on cell type as well as the cell's immediate
156 microenvironment [19, 20]. To determine the functional importance of β1 integrin signaling in our 3D

157 culture model, PDAC clusters were grown for 7 days and treated with either solubilized rat
158 immunoglobulin G (IgG) or a β1 integrin neutralizing antibody [Supplementary Table 1] for 4 days.
159 Because antibodies are targeted to an extracellular epitope, and are unable to cross the cell membrane,
160 the β1 integrin neutralizing antibody specifically blocks β1 integrin outside-in signaling. Following
161 administration of either IgG or β1 integrin neutralizing antibody, cells were fixed, sectioned
162 histologically, and analyzed.

163

164 After 4 days of treatment with control IgG, brightfield microscopy of PDAC clusters showed distinct
165 colonies with smooth and ordered interactions with the surrounding Matrigel (Fig. 6a). In contrast, β1
166 integrin blockade induced structural disorder of PDAC clusters, disrupting their interaction with
167 surrounding Matrigel as well as induced some disintegration of clusters, as evidenced by an increase in
168 scattered, single cells (Fig. 6b). Upon histological analysis, PDAC clusters treated with IgG formed
169 organized colonies with 1 or multiple lumen (Fig. 6 c-f); conversely, β1 integrin blockade abrogated
170 lumen formation (Fig. 6 g-j), suggesting that β1 integrin outside-in signaling is necessary for PDAC
171 cell:cell adhesion and formation of higher ordered 3D structure. Moreover, β1 integrin blockade
172 affected E-cadherin (ECAD) expression at the cell membrane. PDAC clusters in the treated group showed
173 punctate, noncontiguous staining, indicating disruption of ECAD localization to cell membranes (Fig 6d-f,
174 h-j).

175

176 We then evaluated the effects of β1 integrin blockade on Kras* effector signaling. Following
177 administration of control IgG, PDAC clusters demonstrated activation of MAPK and PI3K signaling in
178 Matrigel-adjacent and non-Matrigel-adjacent cells indicated by positive staining of pERK and pS6 (Fig. 7
179 b, l, Supplementary fig. 4). Strikingly, following β1 integrin blockade, Kras* effector signaling was

180 restricted to Matrigel-adjacent cells (Fig. 7 g, q). Though β1-integrin-blocked PDAC clusters showed
181 some localization of β1 integrin to the ECM (Fig. 7 h, r), colocalization of β1 integrin and pERK or pS6
182 signals was rare (Fig. 7 i, s). These results suggest that β1 integrin signaling is necessary for PDAC
183 upregulation of Kras* downstream signaling in the absence of ECM signaling in our system.
184 Furthermore, β1 integrin outside-in signaling is dispensable for Kras* effector signaling, if cells are
185 physically adjacent to the ECM.

186

187 **Dual blockade of MEK and β1 integrin synergize to induce cancer cell death**

188 Prior studies have demonstrated that epithelial cell lumen formation is an active process that requires
189 both cell:cell adhesion and cell:ECM signaling. Since lumen formation appears to be protective for PDAC
190 cells in the context of MEK inhibition (Fig. 4d, 5b) and β1 integrin was necessary for lumen formation in
191 our model (Fig. 6g-j), we hypothesized β1 integrin signaling blockade would prevent lumen formation
192 and potentiate the ability of MEK inhibition to induce apoptosis. To test this, PDAC cells were grown in
193 3D for 7 days and treated for 4 days with vehicle (DMSO+IgG), MEK-T, an anti-β1 integrin neutralizing
194 antibody, or a combination of the compounds. Subsequently, PDAC clusters were fixed, sectioned and
195 prepared for immunofluorescence to examine CC3 or TUNEL staining. Singular administration of either
196 MEK-T or anti-β1 integrin neutralizing antibody increased apoptosis, as indicated by increased CC3
197 staining, compared to the vehicle group (Fig. 8a-p, Supplementary Fig. 6). Furthermore, dual inhibition
198 led to significantly increased apoptosis when compared to singular blockade of either pathway (Fig. 8q).
199 TUNEL staining demonstrated similar findings: singular blockade of either MEK or β1 integrin
200 significantly increased cell death, while clusters in the dual blockade group showed significantly
201 increased death when compared to singular blockade of either pathway (Figure 8r, s). These results,
202 taken together, suggest that β1 integrin signaling mediates PDAC resistance to MEK inhibition.

203

204 **Discussion**

205 Our results show that MEK inhibition induced lumen formation in iKras*p53*-mouse-derived PDAC cells
206 *in vitro*. Furthermore, the presence of Cleaved Caspase 3 and TUNEL positive cells in the lumen
207 suggested that MEK inhibition sensitized PDAC cells to anoikis, programmed cell death in response to
208 detachment from the ECM [24]. Cell:cell adhesion and ECM:cell are key signaling networks that may
209 regulate PDAC progression [21-23]. Elucidation of these pathways may provide insight into mechanisms
210 that regulate disease persistence, which would ideally lead to practical, effective molecular targeting
211 and reduction of PDAC burden. Given that ECM-adjacent PDAC cells displayed a survival advantage in
212 the context of MAPK inhibition, we sought to characterize the role of ECM:cell signaling in our system.
213 We hypothesized that β1 integrin played an important role in the survival of ECM-adjacent PDAC cells.

214

215 The integrin family of cell adhesion receptors mediates a multitude of cellular functions crucial to the
216 initiation, progression and metastasis of solid tumors [25]. In human breast cancer, overexpression of β1
217 integrin is correlated with poor prognosis [26, 27], and in vitro β1 blockade induced apoptosis of
218 malignant cells [28]. In pancreatic cancer, overexpression of β1 is correlated with poorer disease-free
219 survival [29]. In a murine model of pancreatic β cell cancer, genetic ablation of β1 integrin led to
220 reduced tumor cell proliferation and senescence [30]. Pancreatic cancer cell lines overexpress integrin α
221 subunits 1-6 and β subunits; moreover, the β1 subunit is found to be constitutively active, mediating
222 adhesion and invasiveness in some PDAC lines [31]. In our study, we found that lumen formation as well
223 as PDAC cell survival in the context of MEK inhibition were significantly decreased following β1 integrin
224 neutralizing antibody administration, suggesting that PDAC resistance to MEK inhibition is mediated in
225 part by β1 integrin signaling.

226

227 Strikingly, singular blockade of β1 integrin decreased Kras* effector signaling in cells lacking ECM
228 attachment but failed to decrease MAPK or PI3K signaling pathway activation in Matrigel-adjacent PDAC
229 cells. These data suggest two novel findings in relation to iKras*p53* PDAC cell biology in vitro. First,
230 cells lacking ECM interaction require β1 integrin to upregulate downstream effectors of Kras*. This is
231 consistent with previous findings that β1 integrin is involved in ERK signaling in PDAC [33] and inhibition
232 promotes central necrosis [34]. The combination therapy likely exacerbated apoptosis due to β1
233 integrin's ability to activate PI3K signaling in PDAC [35]. Furthermore, β1 integrin has be shown to be
234 necessary to activate PI3K when MEK is inhibited [36] and PI3K inhibition produces central necrosis in a
235 pattern similar to our data [37]. The second conclusion drawn from our data suggest that ECM-adjacent
236 cells upregulate Kras*-effector signaling in a β1 integrin-signaling-independent manner. One likely
237 mechanism to explain this is β5 integrin signaling (Figure 7u). β5 integrin is present in PDAC [35] and can
238 activate MEK signaling in breast cancer [38]. Upon β5 integrin inhibition in breast cancer, proliferation is
239 decreased [38]. Lastly, suppression of a specific heterodimer containing β5 integrin (α5β5) in colon
240 cancer increases the function of a heterodimer containing β1 [34]. This crosstalk between β1 and β5
241 integrins suggest that β5 integrin could upregulate Kras-effector signaling in ECM-adjacent cells when β1
242 integrin is inhibited. However, future tests will need to be done to examine the role of β5 integrin in
243 PDAC as well characterizing how subunit-specific signaling may modulate different characteristics of
244 PDAC interaction with the microenvironment, subsequently regulating PDAC cell survival.

245

246 **Methods**

247 **Murine PDAC model and establishment of primary cell cultures**

248 PDAC tumor cell lines from iKras*p53* mice were established as previously described [12]. p48-Cre
249 (Ptf1a-Cre) mice were crossed with TetO-KrasG12D, Rosa26rtTa/rtTa and p53R172H/+ mice to generate
250 p48Cre [38]; TetO-KrasG12D [38, 39]; Rosa26rtTa/+ [38-40]; p53R172H/+ [38-41] (iKras*p53*) mice. In
251 adult mice, DOX was administered through the drinking water, at a concentration of 0.2g/L in a solution
252 of 5% sucrose, and replaced every 3–4 days. Three days following DOX administration, pancreatitis was
253 induced through two series of eight hourly intraperitoneal injections of caerulein (Sigma C9026), at a
254 concentration of 75 µg/kg, over a 48-hour period, as previously described. Following endogenous tumor
255 formation, tissue was harvested from the primary tumor, minced, and digested with 1 mg/ml
256 collagenase V (Sigma) at 37°C for 15 minutes. RPMI-1640 (Gibco) +10% Fetal Bovine Serum +1%
257 penicillin/streptomycin was used to halt digestion and cells were isolated by filtration through a 100 um
258 cell strainer and plated in complete medium containing DOX (Sigma) at 1 µg/mL [40].

259

260 **Cell culture**

261 iKras*p53* PDAC cells were maintained and passaged in 2D culture in IMDM media +10%FBS +DOX
262 1µg/mL. The 3D assay used was adapted from multiple models [14, 42, 43]. Four-well chamber slides
263 (Corning 354104) were coated with 50-100µL Growth-Factor-Reduced (GFR) Matrigel. Afterward, the
264 slides were incubated for 10 minutes at 37°C to induce solidification of GFR Matrigel. PDAC cells were
265 trypsinized and centrifuged. Pellets were resuspended in single-cell-suspension in Waymouth's media
266 (Gibco 11220-035) +10% Fetal Bovine Serum (Gibco 10438-036) + 1% penicillin/streptomycin (Gibco
267 15140-122) and the solution was added atop the GFR Matrigel surface. Every 2-3 days, media was
268 changed. In experiments using small molecule inhibitors, inhibitors were solubilized in DMSO or 1x PBS,
269 and vehicle or drug treatment groups were administered in either technical duplicate or triplicate.
270 Representative experiments of at least 3 biological replicates has been shown unless otherwise noted.

271

272 **Fixation and staining**

273 PDAC clusters were fixed in formalin at 22°C for at least 2 hours. After fixation, chambers from chamber
274 slides were removed, and PDAC clusters in GFR Matrigel were collected and placed in a cryomold
275 (Sakura 4557) with Histogel (Thermo Scientific HG-4000-012) [44]. These samples were then processed,
276 embedded in paraffin, and cut into 5μm-thick sections. The primary antibodies were added and then
277 antigen retrieval was accomplished using the respective antibodies and concentrations seen in
278 Supplementary Table 1. Histology and immunofluorescence analysis were performed as described
279 below.

280

281 ***Brightfield and Cleaved-Caspase 3 Imaging and Quantification***

282 Brightfield and fluorescent images were acquired with an Olympus BX-51 microscope DP71 digital
283 camera/software as well as Pannoramic SCAN II slide scanner and software. Brightfield, low-
284 magnification images of clusters growing in chamber slides were used to quantify PDAC cluster area.
285 Pictures of at least 5 non-overlapping areas were taken and a blinded observer used ImageJ to trace and
286 measure cluster area. Results indicate the average area of at least 100 unique clusters per treatment
287 group. To quantify cleaved-caspase 3 positivity, a blinded observer analyzed cross sections of fixed,
288 sectioned, and stained PDAC clusters. The number of nuclei as well as positive and negative staining was
289 recorded in at least 50 cross sections of unique PDAC cell clusters from 3 biological replicate
290 experiments.

291

292 **TUNEL Staining and Quantification**

293 The sections from two biological replicate experiments were stained using a Terminal deoxynucleotidyl
294 transferase (TdT) dUTP Nick-End Labeling (TUNEL) assay (Millipore S7165), according to the
295 manufacturer's instructions. The slides were deparaffinized, pretreated, and antigen retrieval was done
296 by first using a TdT enzyme and then a rhodamine antibody solution. DAPI was used as a nuclear
297 counterstain. Images of the fluorescently labelled sections were obtained using a Leica SP5X Upright
298 Two-Photon Confocal Microscope. To quantify TUNEL positivity, the number of TUNEL positive nuclei
299 were obtained as well as total number of nuclei per cell cluster.

300

301 **Acknowledgments.** We thank Carlos Espinoza and Daniel Long for technical supports. We thank all the
302 members of the PanTErA (Pancreatic Tumor Eradication Association) at the University of Michigan for
303 constructive suggestions and feedback. We thank Drs Benjamin L Allen, Elizabeth Lawlor and Ron Koenig
304 for serving of Dr Brannon's thesis committee and for sharing their expertise and input on this project.
305 **Funding**: This work was supported by the Cancer Moonshot Initiative (U01CA-224145) to MPM and HCC.
306 This project was also supported by NIH/NCI grants R01CA151588, R01CA198074, the University of
307 Michigan Cancer Center Support Grant (NCI P30CA046592) and the American Cancer Society to MPM
308 and F31CA203563 to ABIII. This project was also supported by 3-P30-CA-046592-28-S2 (Administrative
309 Supplement to the Cancer Center Core Grant) to HCC and MPdM. NS is a recipient of the American
310 Cancer Society Postdoctoral Award. The funders had no role in study design, data collection and
311 analysis, decision to publish, or preparation of the manuscript. This work was made possible by the
312 Tissue and Molecular Pathology Shared resource at the Rogel Cancer Center.

313

314 **Competing Interests**

315 Funding was obtained from the following grants: American Cancer Society, NIH P30CA46592, NIH
316 R01CA151588, NIH R01CA198074, NIH U01CA224145.

317 **References**

318 1 Adamska A, Domenichini A, Falasca M. Pancreatic Ductal Adenocarcinoma: Current and Evolving
319 Therapies. Int J Mol Sci 2017; 18.

320 2 Rahib L, Smith BD, Aizenberg R, Rosenzweig AB, Fleshman JM, Matrisian LM. Projecting cancer
321 incidence and deaths to 2030: the unexpected burden of thyroid, liver, and pancreas cancers in the
322 United States. Cancer Res 2014; 74: 2913–2921.

323 3 Biankin AV, Waddell N, Kassahn KS, Gingras M-C, Muthuswamy LB, Johns AL et al. Pancreatic cancer
324 genomes reveal aberrations in axon guidance pathway genes. Nature 2012; 491: 399–405.

325 4 Bournet B, Muscari F, Buscail C, Assenat E, Barthet M, Hammel P et al. KRAS G12D Mutation
326 Subtype Is A Prognostic Factor for Advanced Pancreatic Adenocarcinoma. Clin Transl Gastroenterol
327 2016; 7: e157.

328 5 McCubrey JA, Steelman LS, Chappell WH, Abrams SL, Wong EWT, Chang F et al. Roles of the
329 Raf/MEK/ERK pathway in cell growth, malignant transformation and drug resistance. Biochim
330 Biophys Acta 2007; 1773: 1263–1284.

331 6 Cox AD, Fesik SW, Kimmelman AC, Luo J, Der CJ. Drugging the undruggable RAS: Mission possible?
332 Nat Rev Drug Discov 2014; 13: 828–851.

333 7 Liu F, Yang X, Geng M, Huang M. Targeting ERK, an Achilles' Heel of the MAPK pathway, in cancer
334 therapy. Acta Pharm Sin B 2018; 8: 552–562.

335 8 Collins MA, Yan W, Sebolt-Leopold JS, Pasca di Magliano M. MAPK signaling is required for

336 dedifferentiation of acinar cells and development of pancreatic intraepithelial neoplasia in mice.
337 Gastroenterology 2014; 146: 822–834.e7.

338 9 Alagesan B, Contino G, Guimaraes AR, Corcoran RB, Deshpande V, Wojtkiewicz GR et al. Combined
339 MEK and PI3K inhibition in a mouse model of pancreatic cancer. Clin Cancer Res 2015; 21: 396–404.

340 10 Infante JR, Somer BG, Park JO, Li C-P, Scheulen ME, Kasubhai SM et al. A randomised, double-blind,
341 placebo-controlled trial of trametinib, an oral MEK inhibitor, in combination with gemcitabine for
342 patients with untreated metastatic adenocarcinoma of the pancreas. Eur J Cancer 2014; 50: 2072–
343 2081.

344 11 Junttila MR, Devasthali V, Cheng JH, Castillo J, Metcalfe C, Clermont AC et al. Modeling targeted
345 inhibition of MEK and PI3 kinase in human pancreatic cancer. Mol Cancer Ther 2015; 14: 40–47.

346 12 Collins MA, Bednar F, Zhang Y, Brisset J-C, Galbán S, Galbán CJ et al. Oncogenic Kras is required for
347 both the initiation and maintenance of pancreatic cancer in mice. J Clin Invest 2012; 122: 639–653.

348 13 Collins MA, Brisset J-C, Zhang Y, Bednar F, Pierre J, Heist KA et al. Metastatic pancreatic cancer is
349 dependent on oncogenic Kras in mice. PLoS One 2012; 7: e49707.

350 14 Lee GY, Kenny PA, Lee EH, Bissell MJ. Three-dimensional culture models of normal and malignant
351 breast epithelial cells. Nat Methods 2007; 4: 359–365.

352 15 Viale A, Pettazzoni P, Lyssiotis CA, Ying H, Sánchez N, Marchesini M et al. Oncogene ablation-
353 resistant pancreatic cancer cells depend on mitochondrial function. Nature 2014; 514: 628–632.

354 16 Paoli P, Giannoni E, Chiarugi P. Anoikis molecular pathways and its role in cancer progression.
355 Biochim Biophys Acta 2013; 1833: 3481–3498.

356 17 Cooper J, Giancotti FG. Integrin Signaling in Cancer: Mechanotransduction, Stemness, Epithelial
357 Plasticity, and Therapeutic Resistance. Cancer Cell 2019; 35: 347–367.

358 18 Bombardelli L, Carpenter ES, Wu AP, Alston N, DelGiorno KE, Crawford HC. Pancreas-specific
359 ablation of beta1 integrin induces tissue degeneration by disrupting acinar cell polarity.
360 Gastroenterology 2010; 138: 2531–40, 2540.e1–4.

361 19 Anderson LR, Owens TW, Naylor MJ. Structural and mechanical functions of integrins. Biophys Rev
362 2014; 6: 203–213.

363 20 Schiller HB, Hermann M-R, Polleux J, Vignaud T, Zanivan S, Friedel CC et al. β1- and αv-class
364 integrins cooperate to regulate myosin II during rigidity sensing of fibronectin-based
365 microenvironments. Nat Cell Biol 2013; 15: 625–636.

366 21 Senthebane DA, Rowe A, Thomford NE, Shipanga H, Munro D, Al Mazeedi MAM et al. The Role of
367 Tumor Microenvironment in Chemoresistance: To Survive, Keep Your Enemies Closer. International
368 Journal of Molecular Sciences. 2017; 18: 1586.

369 22 Venning FA, Wullkopf L, Erler JT. Targeting ECM Disrupts Cancer Progression. Front Oncol 2015; 5:
370 224.

371 23 Lu P, Weaver VM, Werb Z. The extracellular matrix: a dynamic niche in cancer progression. J Cell
372 Biol 2012; 196: 395–406.

373 24 Taddei ML, Giannoni E, Fiaschi T, Chiarugi P. Anoikis: an emerging hallmark in health and diseases. J
374 Pathol 2012; 226: 380–393.

375 25 Desgrosellier JS, Cheresh DA. Integrins in cancer: biological implications and therapeutic
376 opportunities. Nat Rev Cancer 2010; 10: 9–22.

377 26 dos Santos PB, Zanetti JS, Ribeiro-Silva A, Beltrão EIC. Beta 1 integrin predicts survival in breast
378 cancer: a clinicopathological and immunohistochemical study. Diagn Pathol 2012; 7: 104.

379 27 Gonzalez MA, Pinder SE, Wencyk PM, Bell JA, Elston CW, Nicholson RI et al. An
380 immunohistochemical examination of the expression of E-cadherin, α-and β/γ-catenins, and α2-and
381 β1-integrins in invasive breast cancer. J Pathol 1999; 187: 523–529.

382 28 Park CC, Zhang H, Pallavicini M, Gray JW, Baehner F, Park CJ et al. β1Integrin Inhibitory Antibody
383 Induces Apoptosis of Breast Cancer Cells, Inhibits Growth, and Distinguishes Malignant from
384 Normal Phenotype in Three Dimensional Cultures andIn vivo. Cancer Research. 2006; 66: 1526–
385 1535.

386 29 Sun Q, Zhou C, Ma R, Guo Q, Huang H, Hao J et al. Prognostic value of increased integrin-beta 1
387 expression in solid cancers: a meta-analysis. Onco Targets Ther 2018; 11: 1787–1799.

388 30 Kren A, Baeriswyl V, Lehembre F, Wunderlin C, Strittmatter K, Antoniadis H et al. Increased tumor
389 cell dissemination and cellular senescence in the absence of β1-integrin function. The EMBO
390 Journal. 2007; 26: 2832–2842.

391 31 Arao S, Masumoto A, Otsuki M. β1 Integrins Play an Essential Role in Adhesion and Invasion of
392 Pancreatic Carcinoma Cells. Pancreas. 2000; 20: 129–137.

393 32 Sawai H, Okada Y, Funahashi H, et al. Activation of focal adhesion kinase enhances the adhesion
394 and invasion of pancreatic cancer cells via extracellular signal-regulated kinase-1/2 signaling
395 pathway activation. Mol Cancer. 2005;4:37.

396 33 Grzesiak JJ, Cao HST, Burton DW, Kaushal S, Vargas F, Clopton P et al. Knockdown of the β1 integrin
397 subunit reduces primary tumor growth and inhibits pancreatic cancer metastasis. Int J Cancer 2011;

398 129: 2905–2915.

399 34 Grzesiak JJ, Ho JC, Moossa AR, Bouvet M. The Integrin-Extracellular Matrix Axis in Pancreatic
400 Cancer. Pancreas 2007; 35(4): 293-301.

401 35 Choi C, Kwon J, Lim S, Helfman DM. Integrin β1, myosin light chain kinase and myosin IIA are
402 required for activation of PI3K-AKT signaling following MEK inhibition in metastatic triple negative
403 breast cancer. Oncotarget. 2016;7(39):63466–63487.

404 36 Muranen T, Selfors LM, Worster DT, et al. Inhibition of PI3K/mTOR leads to adaptive resistance in
405 matrix-attached cancer cells. Cancer Cell 2012; 21(2): 227-239.

406 37 Bianchi-Smiraglia A, Paesante S, Bakin AV. Integrin β5 contributes to the tumorigenic potential of
407 breast cancer cells through the Src-FAK and MEK-ERK signaling pathways. Oncogene.
408 2013;32(25):3049–3058.

409 38 Kawaguchi Y, Cooper B, Gannon M, Ray M, MacDonald RJ, Wright CVE. The role of the
410 transcriptional regulator Ptf1a in converting intestinal to pancreatic progenitors. Nat Genet 2002;
411 32: 128–134.

412 39 Fisher GH, Wellen SL, Klimstra D, Lenczowski JM, Tichelaar JW, Lizak MJ et al. Induction and
413 apoptotic regression of lung adenocarcinomas by regulation of a K-Ras transgene in the presence
414 and absence of tumor suppressor genes. Genes Dev 2001; 15: 3249–3262.

415 40 Belteki G, Haigh J, Kabacs N, Haigh K, Sison K, Costantini F et al. Conditional and inducible transgene
416 expression in mice through the combinatorial use of Cre-mediated recombination and tetracycline
417 induction. Nucleic Acids Res 2005; 33: e51.

418 41 Olive KP, Tuveson DA, Ruhe ZC, Yin B, Willis NA, Bronson RT et al. Mutant p53 gain of function in

419 two mouse models of Li-Fraumeni syndrome. Cell 2004; 119: 847–860.

420 42 Debnath J, Muthuswamy SK, Brugge JS. Morphogenesis and oncogenesis of MCF-10A mammary
421 epithelial acini grown in three-dimensional basement membrane cultures. Methods 2003; 30: 256–
422 268.

423 43 Pinto MP, Jacobsen BM, Horwitz KB. An immunohistochemical method to study breast cancer cell
424 subpopulations and their growth regulation by hormones in three-dimensional cultures. Front
425 Endocrinol 2011; 2: 15.

426 44 Pal A, Kleer CG. Three dimensional cultures: a tool to study normal acinar architecture vs.
427 malignant transformation of breast cells. J Vis Exp 2014.

428

429 **Figure Legends**

430 **Fig. 1** In a 3D culture system, iKras*;p53* cells recapitulate morphologic characteristics of the primary
431 tumor. **a** Schematic describing the genetic model of the iKras*;p53* mouse, wherein administration of
432 doxycycline (DOX) leads to pancreatic-epithelial-cell-specific expression of oncogenic $Kras^{G12D}$
433 (dominant-negative $p53^{R172H}$ is also constitutively expressed in the pancreatic epithelium). PDA were
434 isolated from endogenous tumors arising. **b** Brief description of endogenous primary tumor formation;
435 In adult mice, DOX was administered through the drinking water. Three days following DOX
436 administration, pancreatitis was induced through two series of intraperitoneal injections of caerulein.
437 Following endogenous tumor formation, tissue was harvested from the primary tumor and the cells
438 were isolated and placed in medium containing DOX. **c** Hematoxylin/eosin stain of primary iKras*p53*
439 PDAC tumors. **d** Brightfield images of PDAC cell lines in 2D culture, maintained in doxycycline (1µg/mL)
440 (Kras* on). **e** Hematoxylin/eosin stain of iKras*p53* PDAC cell cross sections, 6 days following plating in
441 the "on-top" 3D system (cells were also maintained in doxycycline (1µg/mL). **f** Brightfield images of
442 iKras*p53* cells plated in 3D in the absence or presence of doxycycline (1µg/mL) (Kras* on or off,
443 respectively), 6 days following plating of cells. **g** Quantification of cluster area size, 6 days following
444 plating thin the absence (black bars) or presence (yellow bars) of doxycycline (1µg/mL). In
445 quantification, at least 100 clusters were traced and quantified in combined duplicate treatment wells.
446 Bars represent average cluster area ± SD. *$p<0.01$ in Student's t test analysis. Scale bars = 50µm; 500µm
447 (low magnification)

448

449 **Fig. 2** iKras*p53* PDAC cells recapitulate oncogenic Kras* effector pathway activation and expression of
450 membrane proteins in vitro. **a** Nuclear visualization with DAPI along with staining for phosphorylated
451 ERK (pERK) species, indicating MAPK activity in primary tumors and iKras*p53* PDAC cells grown in 3D

452 culture for six days. Scale bar: 50µm. **b** Nuclear visualization along with staining for phosphorylated S6
453 ribosomal protein (pS6) in primary tumors and PDAC cells in 3D culture. **c-j** DAPI staining along with
454 visualization of membrane proteins e-cadherin and claudin-18 in primary tumor and PDAC cells in 3D
455 culture.

456

457 **Fig. 3** Kras* effector blockade abrogates Kras*-mediated growth in 3D. **a-b** Brightfield images of
458 iKras*p53* cells plated in 3D given either DMSO or a MEK inhibitor for seven days. Quantification of
459 cluster area, 4 days post treatment; at least 100 clusters per treatment group were analyzed. Bars
460 represent cluster area mean ± SEM. ANOVA statistical analysis; * indicates $p<0.01$ of the cluster area. **c**
461 Quantification of cluster cross sections with a single layer of epithelial cells adjacent to the Matrigel as
462 well as lumen that accounts for >75% of the cluster area. Over 50 cluster cross sections per treatment
463 group were analyzed. Bars represent single layer cluster prevalence per technical replicate, mean ± SEM.
464 ANOVA statistical analysis; * indicates $p<0.01$. **d, e** Quantification of cluster cross sections of human
465 UM5 cell lines and 4668 cell lines. **f, g** Hematoxylin/eosin stains of representative cluster cross sections
466 of of iKras*p53* cells plated in 3D given either DMSO or a MEK inhibitor for seven days. **h, i**
467 Immunohistochemical staining of phosphorylated ERK at Thr202 and Tyr204 (pERK); brown dye indicates
468 positive staining. Scale bars: 50µm.

469

470 **Fig. 4** MEK inhibition induces apoptotic lumen formation. iKras*p53* PDAC cells (9805) were grown in
471 3D culture for 6 days and then treated with the MEK inhibitor trametinib (MEK-T) for 4 days (Kras*on
472 the entire experiment). **a, b** Immunofluorescence staining of cleaved caspase 3 (CC3) in red, indicating
473 apoptosis. Scale bar: 100µm. **c** Hematoxylin/eosin staining of representative PDAC cluster cross sections
474 from corresponding treatment groups. Scale bar: 50µm. **d** Quantification of prevalence of PDAC cluster

475 cross sections wherein the lumen accounts for >75% of the cluster and contains CC3- positive debris.
476 Bars represent mean prevalence ±SEM of over 50 cluster cross sections in 3 grouped biological repeat
477 studies. Statistics: student's t test; * indicates p<0.001.

478

479 **Fig. 5** Matrigel-adjacent PDA cells display a survival advantage. iKras*p53* PDAC cells (9805) were
480 grown in 3D culture for 6 days and then treated with the MEK inhibitor trametinib (MEK-T) for 4 days
481 (Kras*on the entire experiment). **a** Representative PDAC cluster cross sections, immunofluorescence
482 staining of type IV collagen (Col4) in red. Scale bar: 50µm. **b** Quantification of the prevalence of non-
483 matrigel-adjacent versus matrigel-adjacent, DAPI-positive nuclei in striped and black bars, respectively.
484 Bars represent mean prevalence ±SEM of over 50 cluster cross sections in 3 grouped biological replicate
485 studies. Statistics: student's t test; * indicates p<0.001.

486

487 **Fig. 6** Beta 1 integrin blockade disrupts membrane dynamics. iKras*p53* 9805 PDAC cells were grown in
488 3D for 7 days and subsequently treated for 4 days with either vehicle IgG or anti-β1 neutralizing
489 antibody (10µg/mL). **a, b** Brightfield, low-magnification microscopy of 9805 PDAC clusters in vitro. Scale
490 bar: 250µm **c, g** Hematoxylin/eosin staining of PDAC clusters cross sections, treated with either control
491 (IgG) or anti-β1 integrin blocking antibody Scale bar: 50µm. **d-f, h-j** Immunofluorescence of PDAC cluster
492 cross sections. Scale bar: 50µm. **d, h** Nuclear visualization with DAPI; **e, i** Stain indicating e-cadherin
493 (ECAD) localization; **f, j** Overlay of DAPI and ECAD channels.

494

495 **Fig. 7** β1 integrin blockade decreases Kras* effector signaling and restricts activation to Matrigel-
496 adjacent cells. iKras*p53* 9805 PDAC cells were grown in 3D for 7 days and subsequently treated for 4

497 days with either vehicle IgG or anti-β1 neutralizing antibody (10µg/mL). **a-e, k-o** Pictured are
498 representative PDAC cluster cross sections of control treated or anti-β1 integrin-treated cells. Scale bar:
499 50µm. **b, g** Clusters were stained for phosphorylated ERK (pERK) species, indicating MAPK activity. **l, q**
500 Staining for phosphorylated S6 ribosomal protein (pS6). **c, h, m, r** Staining for β1 integrin. **d, i, n, s**
501 Overlay of red and green channels. **e, j, o, t** Overlay of DAPI, red, and green channels. **u** Schematic
502 outlining the potential signaling pathways involved in β1 and β5 integrin signaling that are responsible
503 for PDAC cell survival and proliferation.

504

505 **Fig. 8** β1 integrin blockade sensitizes PDA cells to apoptosis. iKras*p53* 9805 PDAC cells were grown in
506 3D for 7 days and subsequently treated for 4 days with vehicle DMSO, trametinib, an anti-β1 neutralizing
507 antibody (10µg/mL), or dual trametinib and anti-β1 neutralizing antibody. **a-d** Hematoxylin/eosin stains
508 of representative cluster cross sections. Scale bar: 50µm. **e-h** Nuclear visualization with DAPI. **i-l**
509 Immunofluorescence staining of cleaved caspase 3 (CC3) in red, indicating apoptosis. **m-p** Overlay of
510 DAPI and CC3 channels. **q** Quantification of CC3-positive nuclei. Bars represent mean prevalence of CC3
511 positivity per defined nucleus ± SEM. At least 50 unique cluster cross sections from 3 biological replicate
512 experiments were analyzed. Statistical analysis: student's t test. n.s.=p>0.05; * indicates p<0.001. **r**
513 Single channel and merged channel images of TUNEL immunofluorescent staining of representative
514 cluster cross sections receiving vehicle, single, or dual treatment. **s** Quantification of TUNEL-positive
515 nuclei. Every dot represents a cluster indicating the percentage of TUNEL positive nuclei within the
516 cluster, whereas the horizontal lines are the median percentages of TUNEL positive nuclei throughout
517 multiple clusters. Statistical analysis: One-way anova with post-hoc analysis. * indicates p<0.005, **
518 indicates p<0.0005. **t** Diagram depicting cluster phenotype upon response to treatment in 3D cell
519 culture. Clusters receiving no treatment will form solid, spheroids. With trametinib administration, cells
520 in the middle of the spheroid will undergo apoptosis leaving a hollow 3D cluster with the remaining

521 living cells attached to the ECM. Clusters receiving the anti-β1 neutralizing antibody will form
522 disorganized clusters with similar preference for ECM attachment. There is an increase in apoptosis in
523 these clusters compared to the control. Clusters receiving dual treatment of trametinib and the anti-β1
524 neutralizing antibody will again form disorganized clusters with a high percentage of the cells
525 undergoing apoptosis.

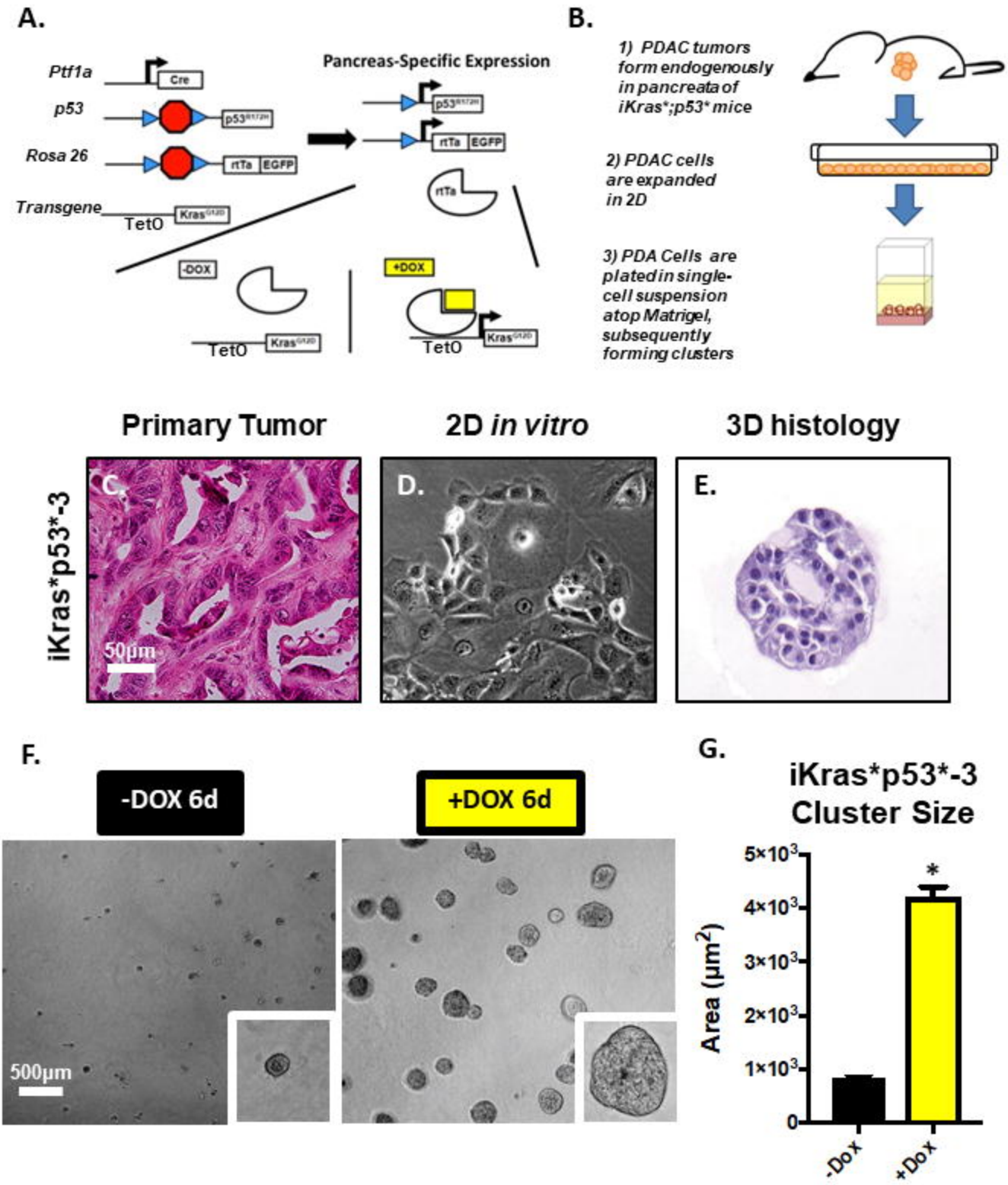
A.
Ptf1a
Cre
p53
Rosa 26
rtTa
EGFP
Transgene
TetO
Pancreas-Specific Expression
-DOX
+DOX
B.
1) PDAC tumors form endogenously in pancreata of iKras*;p53* mice
2) PDAC cells are expanded in 2D
3) PDA Cells are plated in single-cell suspension atop Matrigel, subsequently forming clusters
Primary Tumor
2D in vitro
3D histology
iKras*p53*-3
C.
50µm
D.
E.
F.
-DOX 6d
+DOX 6d
500µm
G.
iKras*p53*-3
Cluster Size
Area (µm²)
5×10³
4×10³
3×10³
2×10³
1×10³
0
*
-Dox
+Dox

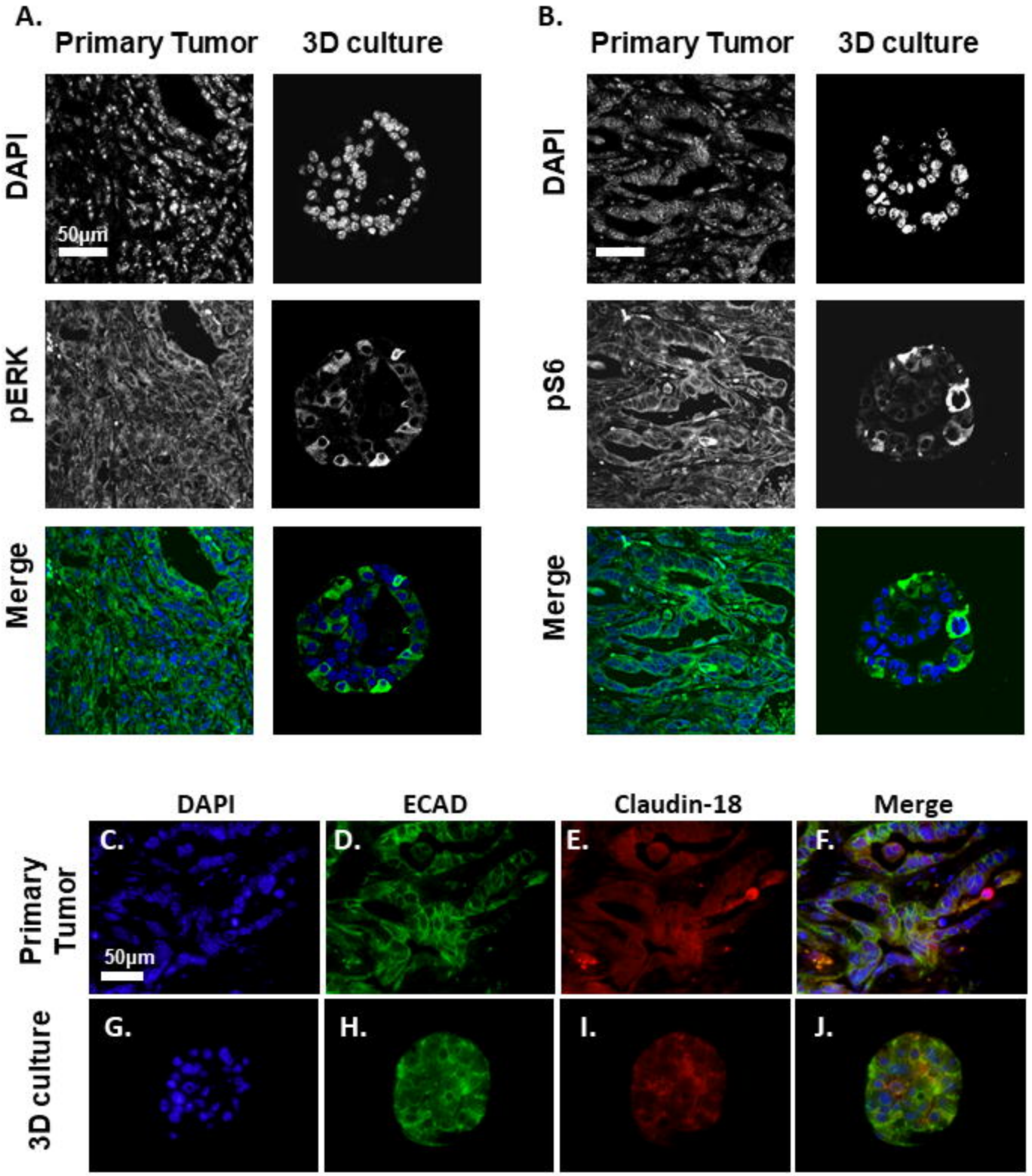
A.
Primary Tumor
3D culture
DAPI
pERK
Merge
50µm
B.
Primary Tumor
3D culture
DAPI
pS6
Merge
DAPI
ECAD
Claudin-18
Merge
Primary Tumor
3D culture
C.
D.
E.
F.
G.
H.
I.
J.
50µm

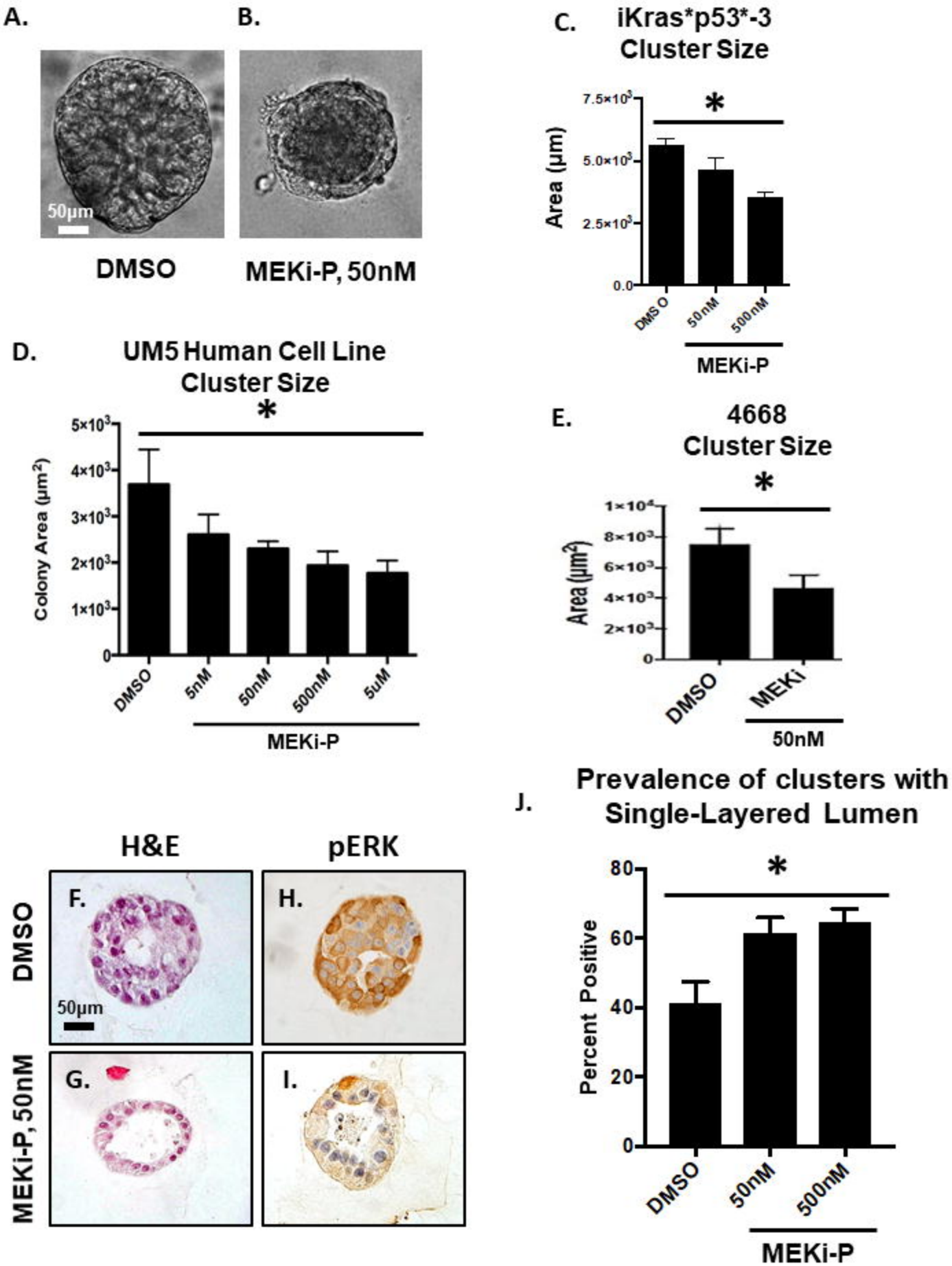
A.
B.
50µm
DMSO
MEKi-P, 50nM
C.
iKras*p53*-3
Cluster Size
Area (µm)
7.5×10³
5.0×10³
2.5×10³
0.0
*
DMSO
50nM
500nM
MEKi-P
D.
UM5 Human Cell Line
Cluster Size
Colony Area (µm²)
5×10³
4×10³
3×10³
2×10³
1×10³
0
*
DMSO
5nM
50nM
500nM
5uM
MEKi-P
E.
4668
Cluster Size
Area (µm²)
1×10⁴
8×10³
6×10³
4×10³
2×10³
0
*
DMSO
MEKi
50nM
H&E
pERK
DMSO
MEKi-P, 50nM
F.
G.
H.
I.
50µm
J.
Prevalence of clusters with
Single-Layered Lumen
Percent Positive
80
60
40
20
0
*
DMSO
50nM
500nM
MEKi-P

A.

DMSO

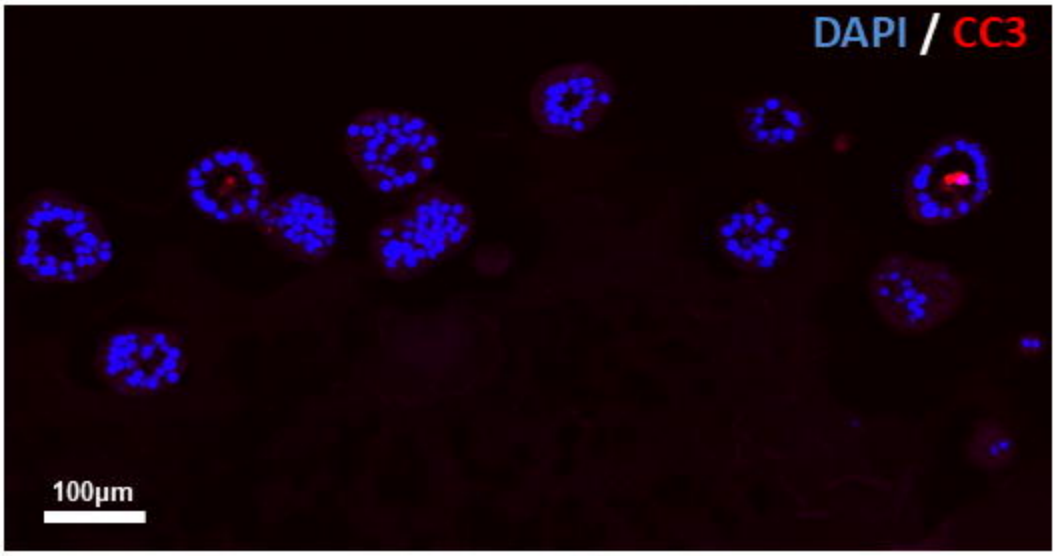

B.

MEKi-T, 1µM

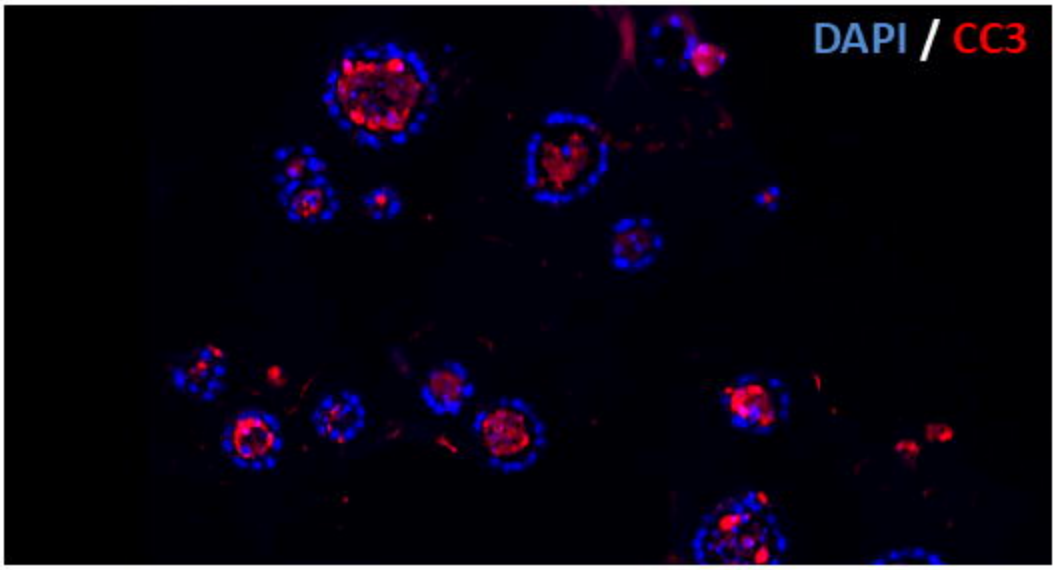

C.

DMSO

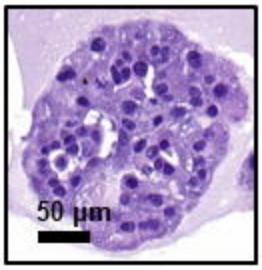

MEKi-T, 1µM

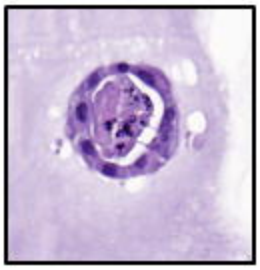

D.

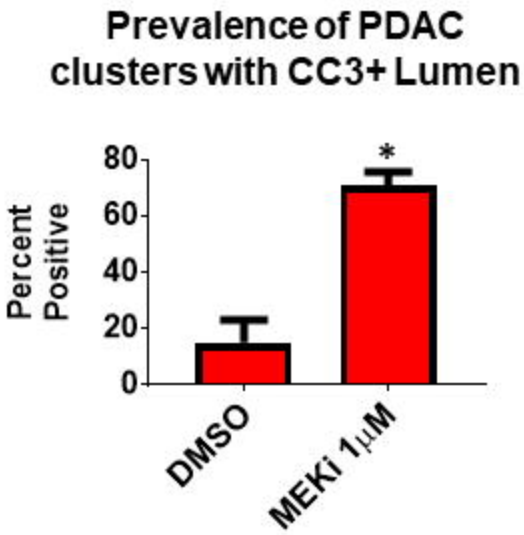

A

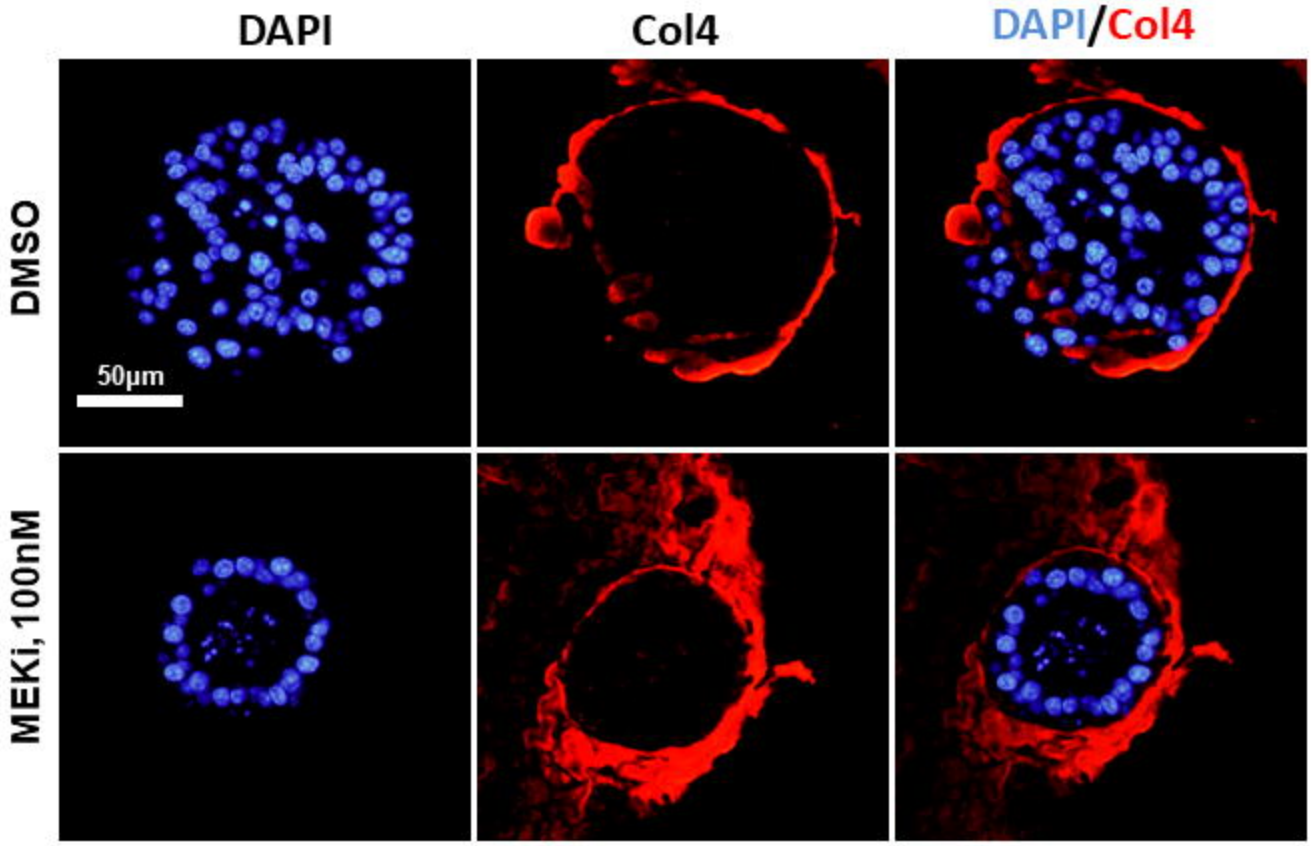
DAPI
Col4
DAPI/Col4
DMSO
MEKi, 100nM
50µm

B

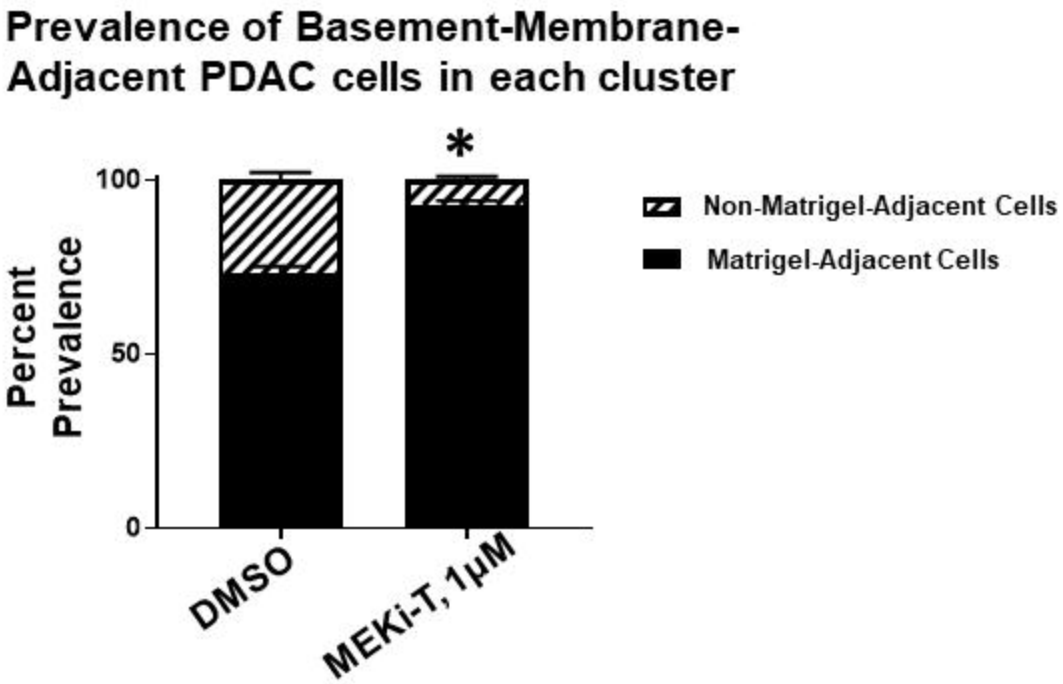
Prevalence of Basement-Membrane-Adjacent PDAC cells in each cluster
*
100
50
0
Percent Prevalence
DMSO
MEKi-T, 1µM
Non-Matrigel-Adjacent Cells
Matrigel-Adjacent Cells

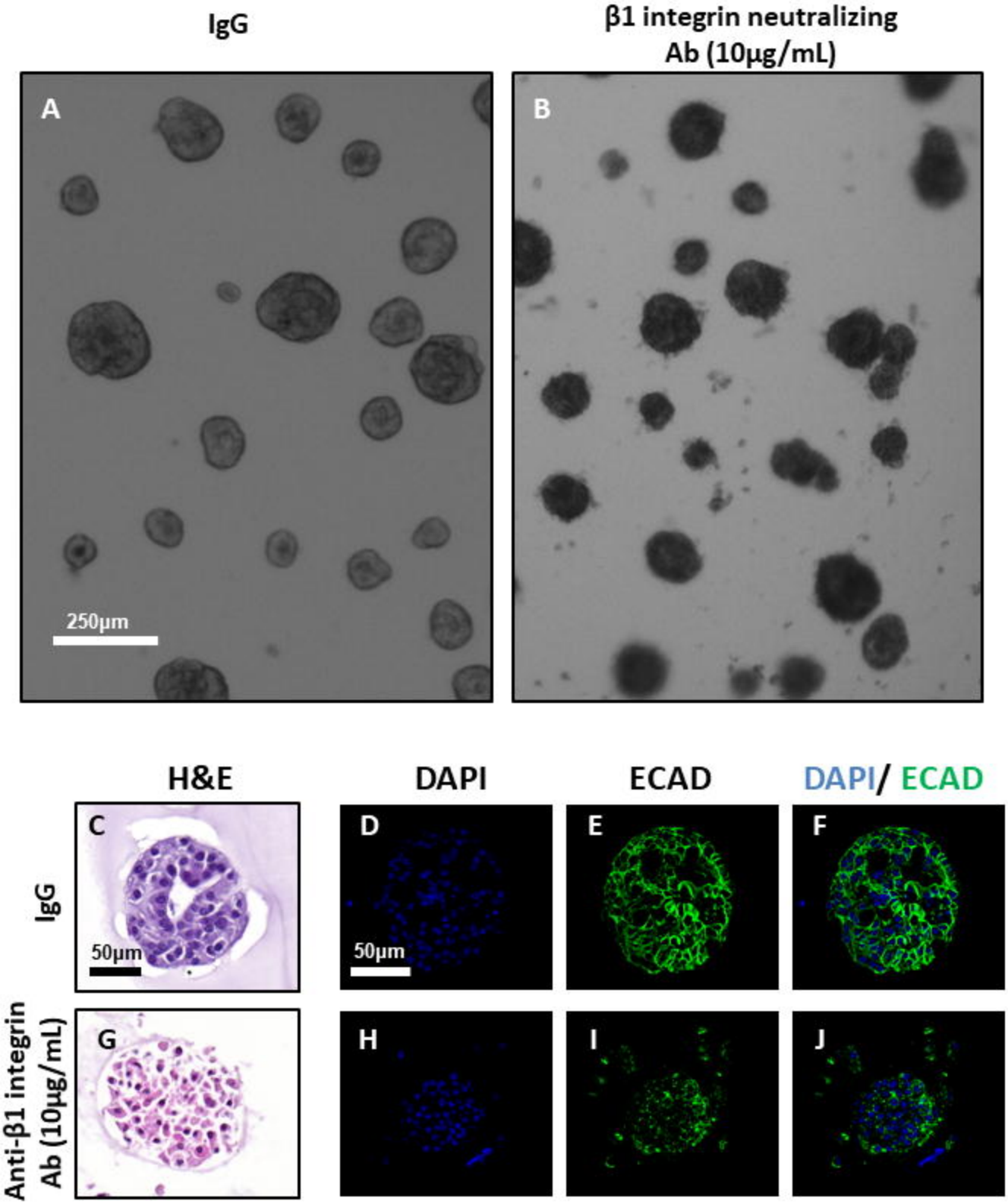
IgG
β1 integrin neutralizing Ab (10µg/mL)
A
B
250µm
H&E
DAPI
ECAD
DAPI/ ECAD
IgG
Anti-β1 integrin Ab (10µg/mL)
C
D
E
F
G
H
I
J
50µm
50µm

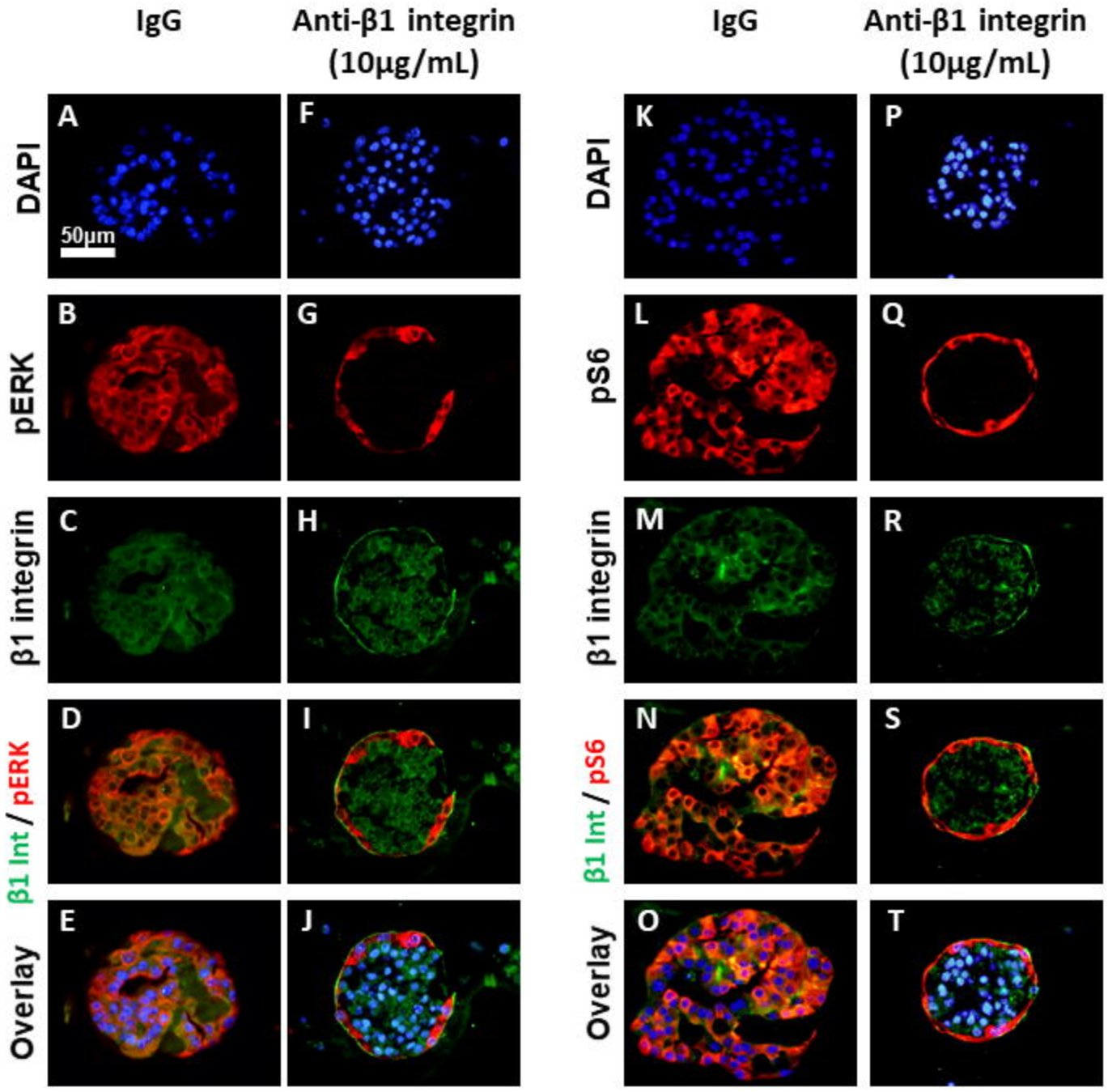
IgG
Anti-β1 integrin (10μg/mL)
IgG
Anti-β1 integrin (10μg/mL)
DAPI
pERK
β1 integrin
β1 Int / pERK
Overlay
DAPI
pS6
β1 integrin
β1 Int / pS6
Overlay
A
B
C
D
E
F
G
H
I
J
K
L
M
N
O
P
Q
R
S
T
50μm

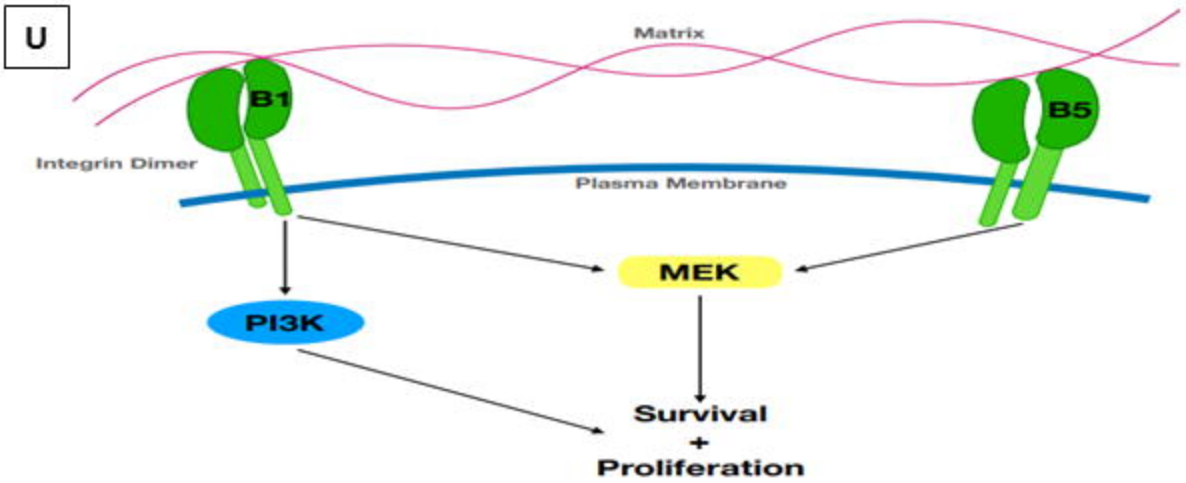
U
Matrix
B1
B5
Integrin Dimer
Plasma Membrane
MEK
PI3K
Survival
+
Proliferation

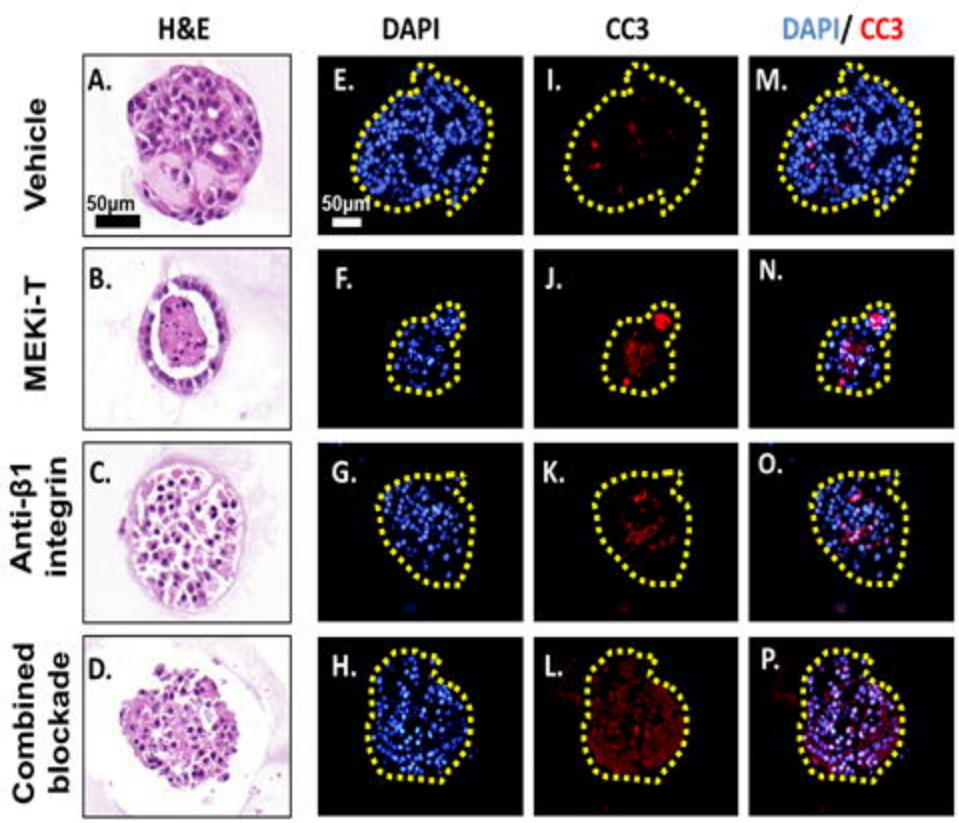
H&E
DAPI
CC3
DAPI/ CC3
Vehicle
MEKi-T
Anti-β1 integrin
Combined blockade
A.
B.
C.
D.
E.
F.
G.
H.
I.
J.
K.
L.
M.
N.
O.
P.
50µm
50µm

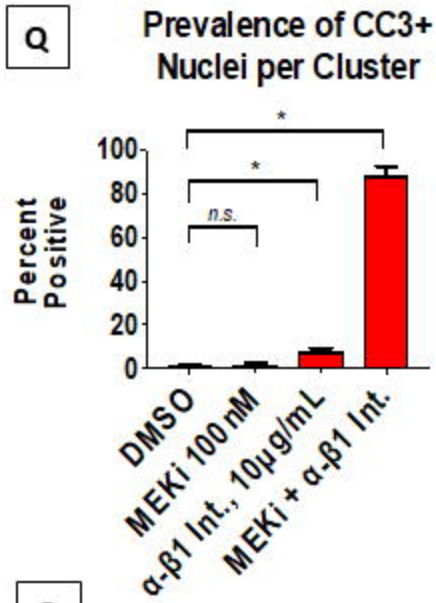
Q
Prevalence of CC3+ Nuclei per Cluster
Percent Positive
100
80
60
40
20
0
*
*
n.s.
DMSO
MEKi 100 nM
α-β1 Int., 10µg/mL
MEKi + α-β1 Int.

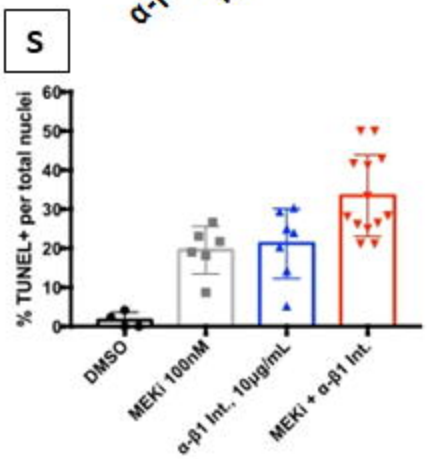
S
% TUNEL+ per total nuclei
60
50
40
30
20
10
0
DMSO
MEKi 100nM
α-β1 Int., 10µg/mL
MEKi + α-β1 Int.

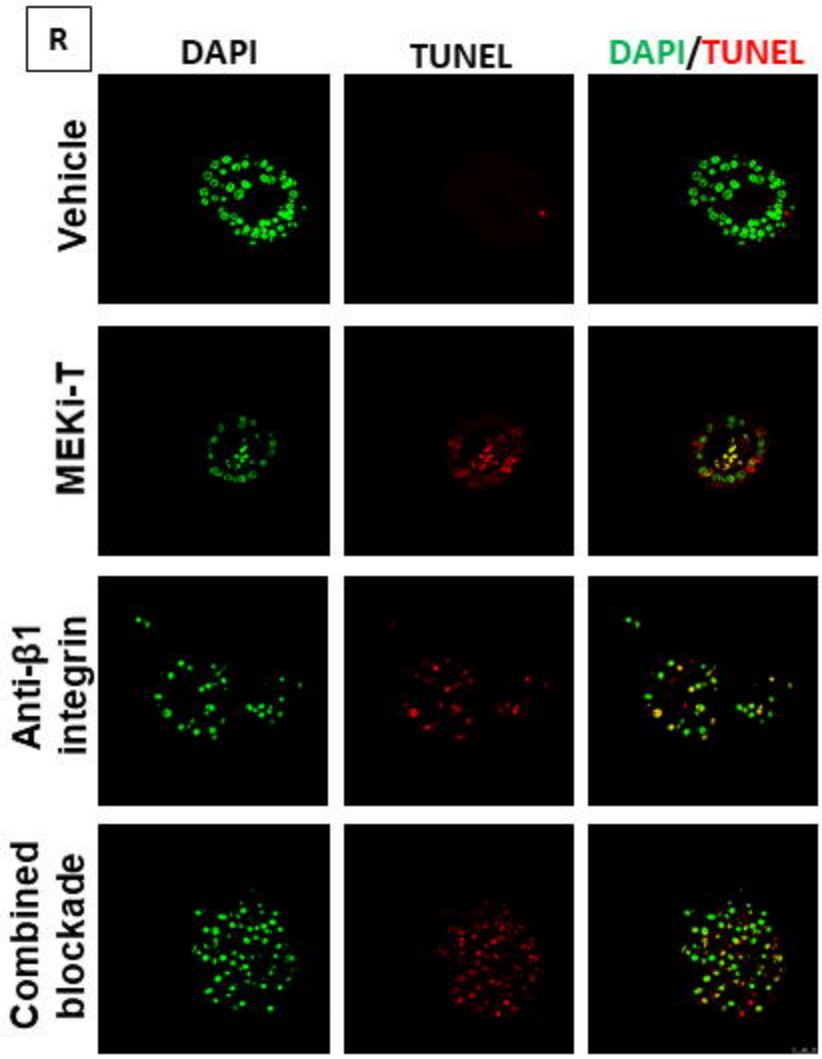
R
DAPI
TUNEL
DAPI/TUNEL
Vehicle
MEKi-T
Anti-β1 integrin
Combined blockade

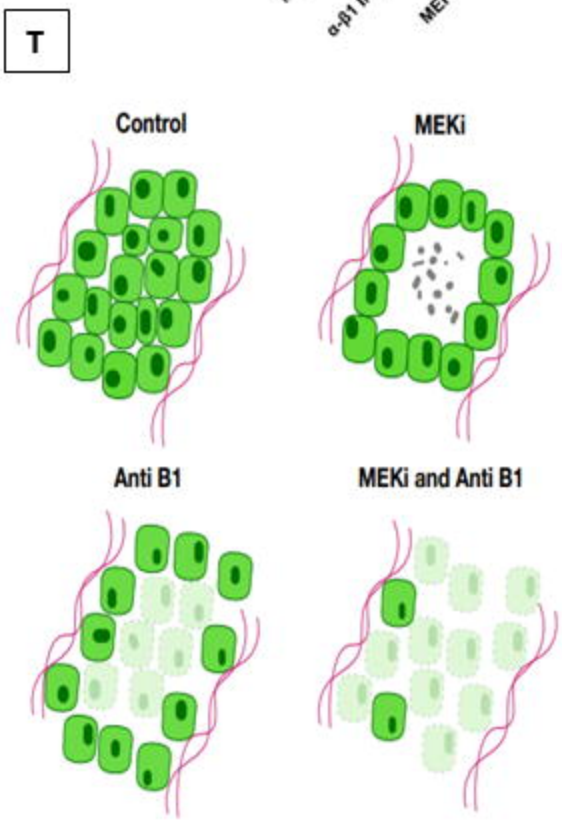
T
Control
MEKi
Anti B1
MEKi and Anti B1